GEOSTANDARDS and GEOANALYTICAL RESEARCH

Iron Isotope Ratios of IAEA B5 Basalt and Whole-Rock Reference Materials (JB-2, BHVO-2, AGV-1, BE-N and RGM-1) Determined by Multi-Collector Inductively Coupled Plasma-Mass Spectrometry

Paolo **Di Giuseppe**, Simone **Vezzoni*** , Stefano **Iannini Lelarge**, Andrea **Rielli**, Samuele **Agostini** and Andrea **Dini**

Consiglio Nazionale delle Ricerche, Istituto di Geoscienze e Georisorse, Via Moruzzi, 1, 56124 Pisa, Italy
* Corresponding author. e-mail: simone.vezzoni@igg.cnr.it

Iron isotopes are increasingly applied in Earth science fields, including cosmochemistry, geochemistry and environmental sciences. Refining non-traditional stable isotope systematics requires well-characterised isotopic reference materials to ensure accuracy and precision. Consequently, the direct comparison of data obtained from different laboratories is a key prerequisite for establishing reliable isotopic systematics. Here, we describe a new Fe isotope measurement method using multi-collector-ICP-MS. The Fe isotope ratios of widely used geological reference materials (JB-2, BHVO-2, BE-N, AGV-1 and RGM-1) were measured and new Fe isotope values for IAEA-B5 (basalt from Mount Etna, Italy) are recommended. Anion exchange chromatography was used to separate Fe from the rest of the matrix. Mass bias was corrected using a standard-sample-standard bracketing method combined with Ni-doping. Iron isotope ratios of JB-2, BHVO-2, BE-N, AGV-1 and RGM-1 show strong agreement with published values and fall within reported analytical uncertainties. Based on these results, we validate and propose $\delta^{56}Fe = 0.103 \pm 0.064$ (2*s*) and $\delta^{57}Fe = 0.141 \pm 0.068$ (2*s*) as recommended values for IAEA-B5. We further advocate the IAEA-B5 as a robust and complementary reference material for analytical validation and quality control in Fe isotope studies, providing both a supplement to and an alternative for established iron isotope reference materials.

Keywords: iron isotopes, reference materials, MC-ICP-MS Neptune Plus, Ni-doping, IAEA-B5.

Received 04 Jun 25 – Accepted 03 Sep 25

Isotope reference materials are essential for calibrating and validating analytical procedures used to determine isotope ratios, ensuring accurate, precise measurements, and enabling inter-laboratory comparisons. Despite the significant advances in isotope ratio measurements, however, the production of isotope reference materials has not kept pace with the growing demand for isotope analysts. Recent progress in multi-collector inductively coupled plasma-mass spectrometry (MC-ICP-MS) now allows for the investigation of non-conventional stable isotopic fractionation across a broad range of elements (e.g., Johnson *et al.* 2004). These features make individual elements susceptible to distinct fractionation mechanisms, thereby defining them as unique tracers for a variety of geological, biological and cosmochemical processes (e.g., Teng *et al.* 2017). Among these, Fe isotopes have gained particular attention due to their potentially significant stable isotope fractionations, which makes isotopic systematics applicable across diverse scientific fields (Beard and Johnson 2004).

Iron is a transition metal element and it represents a major constituent of the Earth's crust, mantle, and by far the more abundant element of terrestrial core. It appears with multiple redox states, buffering the redox state of geological systems (Beard and Johnson 2004, He *et al.* 2015b). Iron has four stable isotopes, ^{54}Fe, ^{56}Fe, ^{57}Fe and ^{58}Fe, with mean natural abundances of 5.845%, 91.754%, 2.119% and 0.282%, respectively (Prohaska *et al.* 2022). Given its

doi: 10.1111/ggr.70017

geochemical properties, high abundance and multivalence states, iron isotope studies are applicable to a wide range of geological processes. This makes iron isotopes a powerful tool for fingerprinting metal sources, assessing biogeochemical reactions that influence iron transport, and providing insights into both low- and high-temperature geological processes. This includes hydrothermal fluid circulations, ore forming, weathering and ocean processes, different *critical zone* (CZ) dynamics, material cycling through the crust and mantle, and processes spanning biological, environmental and cosmochemical contexts (Zhu *et al.* 2000, Rouxel *et al.* 2003, Beard and Johnson 2004, von Blankenburg *et al.* 2008, Dauphas *et al.* 2017).

Precise and accurate isotopic measurements are essential to detect the subtle Fe isotope fractionation in most bio-geological samples. Initial Fe isotope ratio measurements were conducted using thermal ionisation mass spectrometry (Völkening and Papanastassiou 1989), later incorporating a double spike technique for instrumental mass bias correction (e.g., Johnson and Beard 1999). However, early results revealed that TIMS measurements had limited precision (± 0.6‰, 2 standard deviations, 2*s*, for δ^{56}Fe), largely due to difficulties to obtain complete metal ionisation and non-ideal source evaporation conditions (Johnson and Beard 1999, Fantle and Bullen 2009). Over the past three decades, the advent of MC-ICP-MS and improved analytical procedures have enabled highly precise and accurate Fe isotope analyses on geomaterials (Dauphas *et al.* 2017). Among the first results on Fe isotope measurements are those reported by Weyer and Schwieters (2003), which demonstrated significant gains in efficiency and measurement precision (0.1‰ for δ^{56}Fe, 2*s*). Subsequently, several studies using MC-ICP-MS have reported better precision and accuracy (Schoenberg and von Blanckenburg 2005, Dauphas *et al.* 2009, 2017, Millet *et al.* 2012, He *et al.* 2015a, Sossi *et al.* 2015 and references therein), with values down to 0.03‰ on δ^{56}Fe under ideal conditions according to Millet *et al.* (2012) and Chen *et al.* (2017).

Several factors can influence the precision and accuracy achievable with MC-ICP-MS (Albarède and Beard 2004). These include: (i) effective sample digestion and element chemical separation by ion exchange chromatography to completely isolate Fe from the matrix, particularly elements with similar chemical behaviour (e.g., Ni, Cr, Cu), which can introduce matrix effects and isobaric interferences; (ii) resolution of plasma-gas polyatomic interferences from argide species (e.g., $^{40}Ar^{14}N^{+}$ on ^{54}Fe, $^{40}Ar^{16}O$ on ^{56}Fe and $^{40}Ar^{16}OH^{+}$ on ^{57}Fe) and (iii) selecting the optimal mass bias correction method inherent to plasma source mass spectrometry. Compared to chemical preparation, polyatomic ion interferences and instrumental mass bias present the greatest challenges to measurement accuracy and precision (e.g., Belshaw *et al.* 2000, Dauphas *et al.* 2009).

Polyatomic interferences are a major challenge in ICP-MS and the literature offers several strategies to address them. A common approach employs a desolvating nebuliser to increase the Fe/argide ratios, generating a dry plasma with low oxide and hydroxide formations (e.g., Belshaw *et al.* 2000, Zhu *et al.* 2002, Anbar 2004). However, they require nitrogen gas to optimise sensitivity and signal stability, which may introduce nitrogen-based interferences (NO and ArN), and demand high sample loads (up to 40 ppm) to achieve high and constant signal levels (Weyer and Schwieters 2003). Hexapole collision cells have also proven effective in Fe isotope analyses by reducing Ar-based interferences via interaction with an Ar-H_2 gas mixture (e.g., Johnson *et al.* 2002), although new interferences may occasionally arise (e.g., Dauphas *et al.* 2004). Cold plasma (~ 600W, Kehm *et al.* 2003) minimises Ar-based ions by lowering RF power and plasma temperature, but may promote molecular species such as ArN^{+} and $ArOH^{+}$ and/or Ca-based ions like CaO^{+} and $CaOH^{+}$, which interfere with $^{56}Fe^{+}$ and $^{57}Fe^{+}$, respectively (e.g., Beard *et al.* 2003, Dauphas *et al.* 2009). Medium/High Resolution (MR-HR) mode is often considered the most effective approach to separate polyatomic interferences from Fe masses. It can resolve most of the polyatomic interferences on the iron peaks while optimising analytical sensitivity, without the need for desolvating nebulisers or interference suppression techniques, that require low sample concentrations and further dilution steps, that may potentially increase the error of the measurement (Malinovsky *et al.* 2003, Weyer and Schwieters 2003, Poitrasson and Freydier 2005, Schoenberg and von Blankenburg 2005).

Accurate and precise Fe isotope measurements also require the correction of mass bias fractionation. Strategies such as standard-sample bracketing (SSB) involve analysing a certified reference material with known composition to correct sample ratios, assuming instrumental mass bias and matched concentrations and requiring controlled laboratory conditions (He *et al.* 2015a, Dauphas *et al.* 2017).

Another technique, external normalisation (or doping), exploits mass-dependent bias by adding an elements of similar mass, which are commonly Cu or Ni, to correct Fe ratios. Copper (Cu)-doping helps to reduce uncertainty caused by instrumental mass bias instability and mitigates matrix effects, though the inability to simultaneously measure

the masses of ^{63}Cu and ^{65}Cu with Fe ions requires peak jumping in dynamic mode. An additional drawback of Cu-doping is the difficulty of fully removing Cu during chemical purification, especially in Cu-rich samples (e.g., Arnold *et al.* 2004, Dauphas *et al.* 2009, Zhu *et al.* 2018). In contrast, Ni-doping offers the advantage of simultaneous Fe and Ni isotope measurements without requiring peak jumping, and is easier to separate from Fe than Cu during chemical purification, despite possible ^{58}Ni-^{58}Fe interference (Poitrasson and Freydier 2005, Dauphas *et al.* 2009, Gong *et al.* 2020). The double spike method, using ^{57}Fe and ^{58}Fe, is widely considered as the most accurate technique (Malinovsky *et al.* 2003, Millet *et al.* 2012) as it corrects mass bias in real time and is independent of laboratory conditions, achieving accuracy of $2s = 0.02‰$ for $\delta^{56}Fe$ (Millet *et al.* 2012). However, the double-spike technique demands precise high-purity dilutions, time-consuming analysis, and difficulties in correcting the ^{58}Ni-^{58}Fe interferences (Rudge *et al.* 2009, Finlayson *et al.* 2015).

The growing demand within the scientific community for reliable reference materials, combined with the evolution of analytical techniques such as MC-ICP-MS, makes the availability of well-characterised new reference materials essential. In this light, we describe in detail the analytical method set up and present, for the first time, the Fe isotope values of IAEA-B5 basaltic rocks, measured for $\delta^{56}Fe$ and $\delta^{57}Fe$ values relative to IRMM-524b. These are recommended values, offering a valid option for future comparative studies. To achieve this, we first analysed five well-known geological reference materials, chosen for their similar compositions and matrix effects, ranging from basalts (JB-2, BHVO-2 and BE-N) to andesitic and rhyolitic rocks (AGV-1 and RGM-1).

Experimental

High-precision Fe isotope data require meticulous sample digestion and chemical purification. Chemical purification of Fe is strongly linked to the affinity of Fe for chloride complexes and their high partition coefficients on anion exchange resins (Strelow 1980). We performed Fe isotope chemical purification starting from the methodology proposed by Sossi *et al.* (2015), considering that the low volume of reagents used during the procedure allows the possibility to minimise blanks and maximise Fe separation from the matrix. This approach was also followed to further develop the method for potential Zn-Cu separation and isotope measurements. In the next paragraph, we describe the implementations made from the method by Sossi *et al.* (2015) that were mainly targeted to optimise Fe recovery.

Iron isotope ratios of IRMM-524b and other geological reference materials were measured using a (Thermo Scientific) MC-ICP-MS Neptune Plus in the Laboratorio Isotopi Radiogenici e Stabili Non-Convensionali (Radiogenic and Non-Conventional Stable Isotopes Laboratory) at the Istituto di Geoscienze e Georisorse of Consiglio Nazionale delle Ricerche (IGG-CNR) of Pisa, Italy. The complete isotope measurement procedure is described in the following paragraphs. Major element determinations of IAEA-B5 were performed by X-ray fluorescence spectrometry (XRF) at the Dipartimento di Scienze della Terra "Ardito Desio", Università degli Studi di Milano, using WD-XRF Rigaku Supermini 200. Absolute uncertainties in XRF measurements were in the range of 0.2% *m/m* (2*s*), whereas trace element data are available in the literature (Tonarini *et al.* 2003).

Reagents

To obtain ultra-pure de-ionised water, we started with 18.2 MΩ cm resistivity water, further purified by sub-boiling distillation using a SavillexTM DST-1000 system. Concentrated acids, hydrochloric acid (HCl, 37%), nitric acid (HNO_3, 65%) and hydrofluoric acid (HF, 40%) of Normalpur, Suprapur and Ultrapure quality were distilled to produce high-purity HNO_3 (14 mol l^{-1}), HCl (6.6 mol l^{-1}) and HF (23 mol l^{-1}). AG1-X8 (200–400 mesh) anion exchange chromatography resin and ion-exchange columns (Bio-Rad, USA) were used for chemical separation. The resins were rinsed with sub-boiled distilled water and stored in 0.5 mol l^{-1} HCl.

Laboratory cleaning protocol

To prevent contamination, all materials were cleaned with acids. The perfluoroalkoxy alkane (PFA) Savillex vials were subjected to the following cleaning procedure after previous use: they were first immersed in a glass beaker containing *aqua regia* (1:3 molar ratio of HNO_3 and HCl) for a week. They were then rinsed with 1 sub-boiled H_2O, subsequently placed in a beaker filled with HNO_3 and put on a hot plate overnight at 75–85 °C. The next day, the vials were rinsed with 1 sub-boiled H_2O, and filled with HF acid, tightly capped and heated on a hot plate overnight. Finally, they were removed from the hot plate, and after cooling, they were rinsed five times with one sub-boiled H_2O. The 15 ml Falcon test tubes were pre-cleaned before use, through filling with 2% HNO_3, placed on a hotplate at 75 °C overnight, and then rinsed three times with one sub-boiled H_2O.

Sample materials

We used the Fe certified reference material IRMM-524b, provided by the European Institute for Reference Materials and Measurements (IRMM), which consist of high-purity iron wire (99.996%), with Mn and Co as minor impurities. NIST SRM 986 Ni ($^{58}Ni/^{60}Ni$ = 2.596061, $^{61}Ni/^{60}Ni$ = 0.043469 and $^{62}Ni/^{60}Ni$ = 0.138600), used for internal correction, is a certified reference material from the National Institute of Standards and Technology (NIST), containing 0.50 g of nickel metal with a purity of 99.999%. The geological reference materials used in this study include JB-2 (basalt powder, U.S. Geological Survey), BHVO-2 (basalt powder, U.S. Geological Survey), AGV-1 (andesite powder, U.S. Geological Survey), BE-N (basalt powder, CRPG, Centre de Recherches Pétrographiques et Géochimiques), RGM-1 (rhyolite powder, U.S. Geological Survey). For the first time, we additionally measured reference material IAEA-B5 (basalt powder, International Atomic Energy Agency). Major (XRF, this study) and trace elements (ICP-MS, Tonarini *et al.* 2003) of IAEA-B5 are reported in online supporting information Table S1 for a more comprehensive geochemical characterisation.

Sample digestion and chemical separation

All the sample digestion and chemical separation steps were conducted in a class-100 (ISO 5) clean room under a chemical hood. Approximately 2.5 g of Fe certified reference materials IRMM-524b and 0.5 g of Ni certified material NIST SRM 986 were weighed into 30 ml PFA vials. Concentrated HNO_3 (14 mol l^{-1}) was then added, and to achieve complete dissolution, the vials were placed on a hot plate at 75° C for a week. Afterwards, the vials were opened and the samples were dried. Once dried, a calculated aliquot of 2% HNO_3 was added to produce 100 μg g^{-1} concentrated stock solutions for both reference materials.

A different dissolution procedure was used for silicate reference materials. Approximately 30 mg of sample powder was weighed in 15 ml PFA vials and subject to an initial three-day digestion step using a mixture of HF (4 ml, 24 mol l^{-1}) and HNO_3 (1 ml, 14 mol l^{-1}) at 75 °C. After drying, a second HF+HNO_3 (4:1) dissolution step was performed, with vials kept on a hot plate at 75 °C for a week. During this time, samples were placed in an ultrasonic bath for 2–3 min, three to four times per day, to further promote complete dissolution of any eventual residue. The two-steps of HF+HNO_3 treatment were specifically designed to ensure complete dissolution and full breakdown of silicate matrices. When dissolution was completed, the PFA vials were opened and the solutions evaporated to dryness. To remove residual HF and fluorides, the dried samples were re-fluxed with 1 ml concentrated 14 mol l^{-1} HNO_3 and then evaporated to dryness. Then, 5 ml of 6.6 mol l^{-1} HCl was added, and the samples were ultrasonically treated and heated on a hot plate at 75 °C for 24 h until a clear solution was obtained for all the samples. Finally, samples were dried again, redissolved in 2 ml of 6.6 mol l^{-1} HCl, and stored in polypropylene vials, ready for the chemical purification step (Table S2). While the final HCl step resembles that used by Sossi *et al.* (2015), the overall digestion strategy adopted here remains distinct.

To minimise matrix effects, isobaric interferences and isotope fractionation during chemical separation, efficient matrix removal and complete Fe recovery (i.e., > 99%) are essential. For this purpose, PTFE columns (0.4 × 7 cm) were filled with 1 ml BioRad AG1-X8 (200–400 mesh). Pre-cleaning involved flushing with 5 ml 3 mol l^{-1} HNO_3, followed by 5 ml 1 sub-boiled H_2O (Table S2). Columns were then conditioned with 5 ml 6.6 mol l^{-1} HCl before sample loading. Hence, 0.5 ml of 6.6 mol l^{-1} HCl sample solution containing ~ 40 μg of Fe was loaded, during which ferric chlorides appeared as a distinct yellow ring on the resin (Figure S1). Copper and other matrix elements, particularly Ni and Cr, were eluted with a total of 11 ml (7+4) 6.6 mol l^{-1} HCl. Iron was recovered by adding 3 ml 0.5 mol l^{-1} HCl in six 0.5 ml steps, followed by an additional 1.5 ml to check the possible presence of Fe residues after elution. Eluates were dried, re-fluxed with 1 ml concentrated 14 mol l^{-1} HNO_3 and dried again to eliminate any chloride complexes. Subsequently, 1 ml 2% HNO_3 was added, samples were ultrasonically treated and dried once more. This step ensures that the acid molarity is perfectly matched across the samples, reference material and blank solutions, which is essential for achieving accurate isotopic measurements. Finally, the dried Fe residues were dissolved in 8 ml 2% HNO_3 to obtain a sample concentration of ~ 5 μg g^{-1}, ready for measurement by MC-ICP-MS. During chemical processing, the Fe blank was ~ 2 ng, which is negligible for the analysed samples.

Fe isotope ratio measurement

Iron isotope ratios of IRMM-524b and geological reference materials were measured using a Thermo Scientific High Resolution (HR)-MC-ICP-MS Neptune Plus, equipped with an Integrated anti-contamination Enclosure ENC-560 Teledyne CETAC Technologies covering an ASX-560 Teledyne CETAC Technologies automatic autosampler. Samples in 2% HNO_3 solution were introduced using a

100 µl min^{-1} flux cyclonic nebuliser connected to a dual cyclonic spray chamber in quartz, and pared Ni-made skimmer(H-type)/sampling cones. During the measurements, Fe^+ peaks were resolved from ArO^+, $ArOH^+$ and ArN^+ interferences as flat-topped plateaus on the low mass shoulder of argide peaks following the method suggested by Weyer and Schwieters (2003). Measures were performed in high-resolution mode, which provided a mass resolution ($M_{0.95}/M_{0.95}$-$m_{0.05}$) equal to ~ 10000.

Two types of measurement sessions were conducted: (i) a standard-sample bracketing session (SSB) and (ii) a SBB + Ni-doping session. For both protocols, samples and reference material concentrations were matched to within ± 5%. A less concentrated Ni-doped IRMM-524b standard solution (~ 0.5 µg g^{-1}) was used to set up the mass spectrometer, enabling clear differentiation between the real Fe signals and the ones resulting from the isobaric interferences. Before each measurement session, the instrument was left to stabilise for at least 30 min after plasma ignition in a blank solution prior to instrumental tuning and signal intensity optimisation.

In the first sessions, we employed the SSB method without any mass bias correction. During these sessions, we monitored ^{53}Cr, ^{54}(Fe+Cr), ^{56}Fe, ^{57}Fe, ^{58}(Fe+Ni) and ^{60}Ni using Low 4 (L4), Low 2 (L2), Low 1 (L1), Central (C), High 1 (H1) and High 3 (H3), respectively, using 10^{13} Ω, 10^{12} Ω and 10^{13} Ω resistors (Table 1). Measurement protocols varied to assess data quality, with acquisition times of twenty or twenty-five cycles per block for blanks and integration times of 4.194 s per cycle with a 3 s idle. For RMs and samples, the protocol involved forty to sixty cycles in blocks of eight to ten, maintaining the same integration and idle times. A 2% HNO_3 solution was used for washing before and after each blank, RM and sample measurement. ^{53}Cr was monitored to correct for residual ^{54}Cr (isobaric interference on ^{54}Fe), assuming a $^{54}Cr/^{53}Cr$ ratio of 0.2571 (He *et al.* 2014). Tests were conducted using IRMM-524b Fe standard solutions at concentrations of 5 µg g^{-1} and ~ 2 µg g^{-1}, with ^{56}Fe signal in the range of 9.5 and 10 V. Results showed negligible ^{54}Cr, eliminating the need for Cr corrections.

In the following sessions, we applied the standard-sample bracketing plus Ni-doping method. In this protocol, both reference and sample solutions were spiked using NIST SRM 986 with a Fe:Ni ratio of 1:1, following Chen *et al.* (2017), who reported no significant Fe isotope variation when Fe:Ni ratio ranged between 0.5 and 2.0. We recall that using Ni-spiking for mass bias correction offers advantages over other elements (e.g., Cu) due to the simultaneous measurement of Fe and Ni without the need for peak jumping, reducing measurement time and instability (e.g., Arnold *et al.* 2004, Schoenberg and van Blanckenburg 2005). In addition, Ni contained in the sample could be easily separated from Fe during the column separation procedure, ensuring only the Ni added from doping is present in a detectable amount during measurement. In these sessions, ^{54}Fe, ^{56}Fe, ^{57}Fe, ^{58}(Fe+Ni), ^{60}Ni and ^{62}Ni were measured, respectively at Faraday cups Low 4 (L4), Low 3 (L3), Low 1 (L1), Central (C), High 1 (H1) and High 2 (H2), equipped with 10^{12} Ω and 10^{11} Ω resistors with ^{56}Fe intensity between 10 and 11 V using 5 µg g^{-1} concentrated solutions of IRMM-524b Fe (Figure S2). The $^{62}Ni/^{60}Ni$ ratio of 0.138599 was applied for mass bias correction using the exponential law:

$$r = R\left(1 + \frac{\Delta M}{M}\right)^{\beta} \quad (1)$$

where r is the measured isotopic ratio, R is the true ratio, $\Delta M/M$ represents the relative mass difference, and β is the mass fractionation factor (Russell *et al.* 1978, Maréchal *et al.* 1999). Iron isotopes were measured in static mode. To assess reproducibility, accuracy, time efficiency and solution consumption, sample analyses were performed as single, duplicate, triplicate and quintuplet measurements in the bracketing procedure. Sample results were corrected for the consecutive standard mean, from which the blank mean was subtracted. When replicates were measured in sequence, blanks consisted of twenty-five cycles (five blocks of five cycles), while reference materials and samples had sixty or ninety cycles (six blocks of ten cycles or nine blocks of ten cycles) with an integration time of 8.389 s and an idle time of 3 s. For single measurements, blanks, samples and RMs, all used twenty-five cycles with three measurements averaged for the result. A 2% HNO_3 washing solution was used for washing before and after each blank, reference material and sample measurement. An instrumental baseline correction, which consisted of 100 cycles with integration times of 1.02 s, was performed before every sample and RM. Additional modifications, compared with the SSB sessions, included: (i) ensuring Faraday cup alignment within 0.02 amu for precise isotopic mass matching by checking the distance between all the Fe isotope masses taken before interference-free plateau, and more precisely in the middle of the shoulders, (ii) increasing the integration time from 4.194 s to 8.389 s without Fe background rise.

Data are reported in the traditional δ notation relative to IRMM-524b:

Table 1.
Faraday cup configuration, instrumental parameters and operating conditions (MC-ICP-MS Neptune Plus instrument)

SSB Protocol						
Analyte	^{53}Cr	^{54}Fe	^{56}Fe	^{57}Fe	^{58}Fe	^{60}Ni
Cup	L3	L1	C	H1	H2	H4
Amplifier	10^{13} Ω	10^{13} Ω	10^{11} Ω	10^{12} Ω	10^{12} Ω	10^{12} Ω
Coolant gas	1.250 l min^{-1}					
Auxiliary gas	0.85 l min^{-1}					
Nebuliser gas	100 µl min^{-1}					
RF power	1300 W					
Spray chamber	Dual cyclonic quartz					
Sample cone	Ni					
Skimmer cone (H-type)	Ni					
Solution uptake	100 µl min^{-1}					
Washing time	240 s					
Integration time	4.194 s					
Sensitivity	9.5–10 V (^{56}Fe)					
SSB+Ni Doping Protocol						
Analyte	^{54}Fe	^{56}Fe	^{57}Fe	^{58}(Fe+Ni)	^{60}Ni	^{62}Ni
Cup	L4	L2	L1	C	H1	H3
Amplifier	10^{12} Ω	10^{11} Ω	10^{12} Ω	10^{11} Ω	10^{12} Ω	10^{12} Ω
Coolant gas	1.100 l min^{-1}					
Auxiliary gas	0.90 l min^{-1}					
Nebuliser gas	100 µl min^{-1}					
RF power	1300 W					
Spray chamber	Dual cyclonic quartz					
Sample cone	Ni					
Skimmer cone (H-type)	Ni					
Solution uptake	100 µl min^{-1}					
Washing time	90 s					
Integration time	8.389 s					
Sensitivity	11 V (^{56}Fe)					

$$\delta^{x}Fe = \left[\frac{\left(\frac{^{x}Fe}{^{54}Fe}\right)_{sample}}{\left(\frac{^{x}Fe}{^{54}Fe}\right)_{IRMM-524b}} - 1 \right] \quad (2)$$

where x is mass 56 or 57, respectively. A detailed description of Faraday cup configurations and instrumental settings for SSB and SSB+Ni-doping methods is reported in Table 1.

Results and discussion

Standard-sample bracketing (SSB) vs. SSB+Ni-doping

Two diverse measurement protocols using IRMM-524b Fe solution were tested to assess the precision and accuracy of analyses with a 5 µg g^{-1} concentrated solution. Simple standard-sample bracketing (SSB) gave a mean value of $\delta^{56}Fe = 0.041 \pm 0.133$ and $\delta^{57}Fe = -0.003 \pm 0.089$ (2*s*, $n = 31$, Figure 1a). In contrast, the SSB with Ni-doping improved precision, producing lower 2*s* values, with $\delta^{56}Fe = 0.024 \pm 0.061$ (2*s*, $n = 56$) and $\delta^{57}Fe = 0.021 \pm 0.077$ (2*s*, $n = 50$). No significant changes in mean values or errors occurred when using single, duplicate, triplicate or quintuplicate measurements within the bracketing sequence (Figure 1a).

Although Ni-doping enhances precision, it may introduce additional uncertainties, including potential isobaric interferences and the need for mass bias correction. However, the significant difference in natural abundances between ^{58}Ni (~68%) and ^{58}Fe (~0.3%) makes ^{58}Ni-^{58}Fe isobaric interference negligible. Regarding mass bias correction, a strong correlation between exponential coefficients (f_{Fe} *vs.* f_{Ni}, Figure 1b) indicates that Fe and Ni undergo very similar instrumental mass bias, suggesting similar fractionation

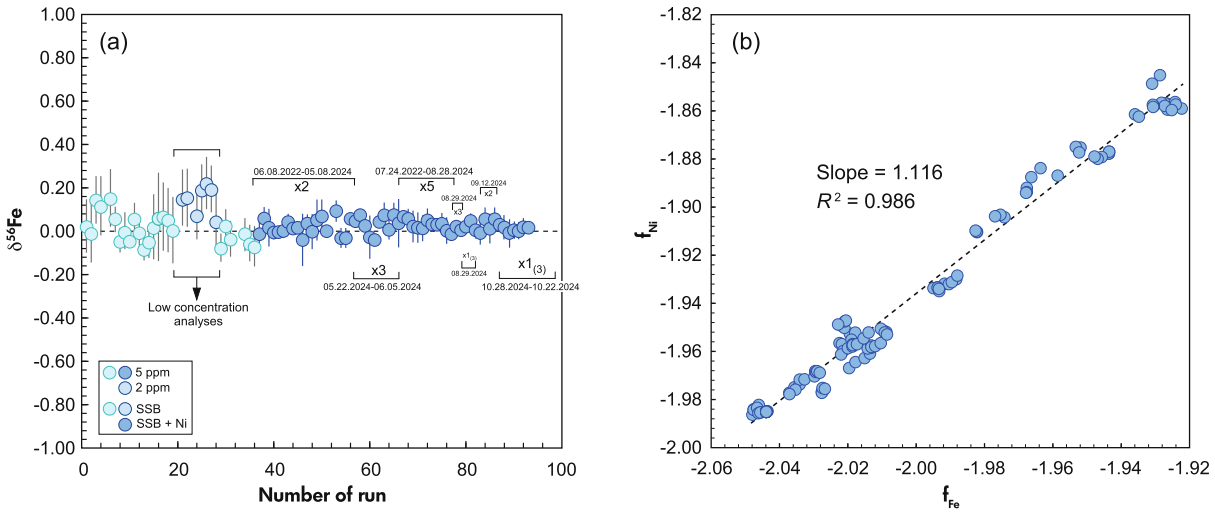

Figure 1. Results of IRMM-524b analyses: (a) intermediate measurement precision of SSB and SSB+Ni methods. Bars on SBB data points represent 2SE (standard error), because single analyses of IRMM-524b were run during bracketing procedure, whereas the bars on SSB+Ni data points represent 2*s* (standard deviation); (b) Plot of measured mass bias fractionation factors over a long term for Fe and Ni isotopic ratios obtaining during SSB+Ni protocol. f_{Fe} and f_{Ni} are relative to $^{56}Fe/^{54}Fe$ and $^{62}Ni/^{60}Ni$ isotopic ratios, respectively with $f_{Fe} = \ln(^{56}Fe/^{54}Fe_{true}/^{56}Fe/^{54}Fe_{measured})/\ln(M^{56}Fe/M^{54}Fe)$ and $f_{Ni} = \ln(^{62}Ni/^{60}Ni_{true}/^{62}Ni/^{60}Ni_{measured})/\ln(M^{62}Ni/M^{60}Ni)$. Theoretical slope (TS) = $\ln(mass^{56}Fe/^{54}Fe)/\ln(mass^{62}Ni/mass^{60}Ni)$. All the measurements carried out during bracketing are reported. ×2, ×3 and ×5 indicate that the sample was measured two, three and five times respectively during the bracketing sequence, whereas $1_{(3)}$ refers to the mean of three single sample measurements.

pathways in the mass spectrometer. The slope of 1.116 and $R^2 = 0.986$ observed in Figure 1b, closely aligns with the theoretical slope (TS = 1.108), calculated using Fe and Ni natural masses, suggesting a consistent fractionation trend. While Fe and Ni exhibit similar geochemical behaviours, slight differences arise due to distinct ionisation potential, as well as solute matrix effects. Instrumental factors, such as instrumental drift over time, plasma conditions, cone wear and sample collection, can influence slope accuracy (e.g., Yin *et al.* 2024). However, the strong agreement between theoretical and experimental slope suggests minimal analytical disturbance from isobaric interferences and instrumental mass bias. This confirms that the use of the Ni doped internal standard method to correct Fe isotope mass fractionation is both feasible and effective (e.g., Chen *et al.* 2017, Chernozhkin *et al.* 2017, González de Vega *et al.* 2020), although this does not mean that the SSB method is invalid. In this light, the use of Ni-doping in our laboratory routine may make the measurements less susceptible to external conditions. Therefore, all the results of geological reference materials presented in this study were obtained using SSB+Ni-doping protocol and following the procedure and instrumental setting described in the previous paragraph.

Fe isotope ratios of geological reference materials

Several replicates of reference materials were measured to test and improve the accuracy of isotopic ratio measurements and to assess the intermediate measurement precision ("external reproducibility") of the MC-ICP-MS method, which is expressed as 2*s* (standard deviation) calculated by the repeated analysis of a given sample processed *n* times (Table 2 and Data Repository (Fe isotope ratios of IAEA-B5 and other reference materials) in Di Giuseppe *et al.* 2025), 2SE (standard error, single analysis), as well as 2SE* ($2SE = 2s/\sqrt{n}$). As previously suggested by Poitrasson and Freydier (2005), when the number of repeated analyses was less than fifteen, Student's *t* factor was used to calculate 2SE* ($2SE^* = [t^{95}*2s] / \sqrt{n}$). This approach yielded 2SE* precisions of ± 0.014 to 0.052‰ for $\delta^{56}Fe$ and ± 0.017 to 0.056‰ for $\delta^{57}Fe$, except for BHVO-2, which showed a higher 2SE of 0.087‰ for $\delta^{57}Fe$.

The $\delta^{56}Fe$ and $\delta^{57}Fe$ isotopic values of geological reference materials measured with Ni-doping internal standard correction are presented in Table 2 and Figures 2 and 3. Comparison between our results and those from the

Table 2.
Mean Fe isotope ratios for geological reference materials

RM	Date	δ^{56}Fe	2*s*	2SE	2SE*	δ^{57}Fe	2*s*	2SE	2SE*	*n*
JB-2	08.05.2024	0.065	0.006			0.077	0.025			2
	08.05.2024	0.124	0.067			0.157	0.069			2
	06.08.2024	0.123	0.076			0.195	0.047			5
	29.08.2024	0.080	0.064			0.104	0.086			3
	29.08.2024	0.126	0.039			0.174	0.061			3
	29.08.2024	0.084		0.057		0.107		0.056		1
	29.08.2024	0.074		0.014		0.131		0.017		1
	Mean	**0.097**	**0.050**		**0.036**	**0.135**	**0.078**		**0.056**	**7**
BHVO-2	06.08.2024	0.164	0.078			0.224	0.057			5
	29.08.2024	0.104	0.089			0.157	0.045			3
	29.08.2024	0.142		0.051		0.238		0.045		1
	29.08.2024	0.113		0.077		0.128		0.060		1
	Mean	**0.131**	**0.047**		**0.050**	**0.187**	**0.092**		**0.087**	**4**
AGV-1	04.06.2024	0.134	0.059			0.247	0.038			3
	04.06.2024	0.131	0.055			0.193	0.032			3
	05.06.2024	0.143	0.044			0.171	0.020			3
	05.06.2024	0.145	0.058			0.149	0.015			3
	06.08.2024	0.153	0.041			0.185	0.036			5
	Mean	**0.141**	**0.016**		**0.014**	**0.189**	**0.065**		**0.055**	**5**
BE-N	29.08.2024	0.166	0.004			0.176	0.019			3
	29.08.2024	0.111		0.041		0.212		0.061		1
	16.10.2024	0.165	0.007			0.199	0.079			$1_{(3)}$
	22.10.2024	0.1483	0.0893			0.2372	0.0764			
	Mean	**0.148**	**0.044**		**0.047**	**0.206**	**0.044**		**0.047**	**4**
RGM-1	27.08.2024	0.186	0.091			0.325	0.104			5
	29.08.2024	0.219	0.029			0.286	0.080			3
	29.08.2024	0.247		0.088		0.315		0.108		1
	16.10.2024	0.258	0.089			0.373	0.088			$1_{(3)}$
	22.10.2024	0.1927	0.085			0.3191	0.0818			
	Mean	**0.221**	**0.057**		**0.052**	**0.324**	**0.056**		**0.050**	**5**
IAEA-B5	25.07.2024	0.129	0.069			0.160	0.015			5
	25.07.2024	0.064	0.084			0.108	0.083			5
	25.07.2024	0.073	0.065			0.149	0.066			5
	25.07.2024	0.088	0.084			0.129	0.071			5
	06.08.2024	0.134	0.043			0.174	0.026			5
	06.08.2024	0.073	0.023			0.126	0.048			5
	12.09.2024	0.102	0.073			0.164	0.006			2
	12.09.2024	0.093	0.042			0.105	0.069			2
	12.09.2024	0.124	0.023			0.193	0.043			2
	12.09.2024	0.134	0.026			0.151	0.006			2
	12.09.2024	0.132	0.018			0.139	0.069			2
	12.09.2024	0.044	0.068			0.060	0.019			2
	12.09.2024	0.152	0.061			0.168	0.029			2
	16.10.2024	0.073	0.035			0.122	0.087			$1_{(3)}$
	16.10.2024	0.126	0.047			0.201	0.093			$1_{(3)}$
	22.10.2024	0.129	0.019			0.157	0.002			$1_{(3)}$
	22.10.2024	0.112	0.051			0.194	0.036			$1_{(3)}$
	Mean	**0.105**	**0.061**		**0.015**	**0.147**	**0.071**		**0.017**	**17**

2*s* is 2 standard deviations
* indicates 2 Standard Error (2SE) calculated using 2*s* and the number of analyses *n*
n is the number of measurements during the bracketing sequence
n in bold is the number of total measurements for each reference material

literature are reported in Table S3. The reference materials analysed in this study included basaltic rocks (JB-2, BHVO-2 and BE-N) and andesitic (AGV-1) to rhyolitic (RGM-1) samples. More evolved igneous rocks displayed heavier isotope enrichment, as previously observed by Dauphas *et al.* (2004), Craddock and Dauphas (2011) and He *et al.* (2015a).

The mean δ^{56}Fe and δ^{57}Fe values of JB-2 were 0.097 ± 0.050‰ (2*s*, $n = 7$) and 0.135 ± 0.078‰ (2*s*, $n = 7$), respectively, in agreement with values of 0.110 ± 0.032‰

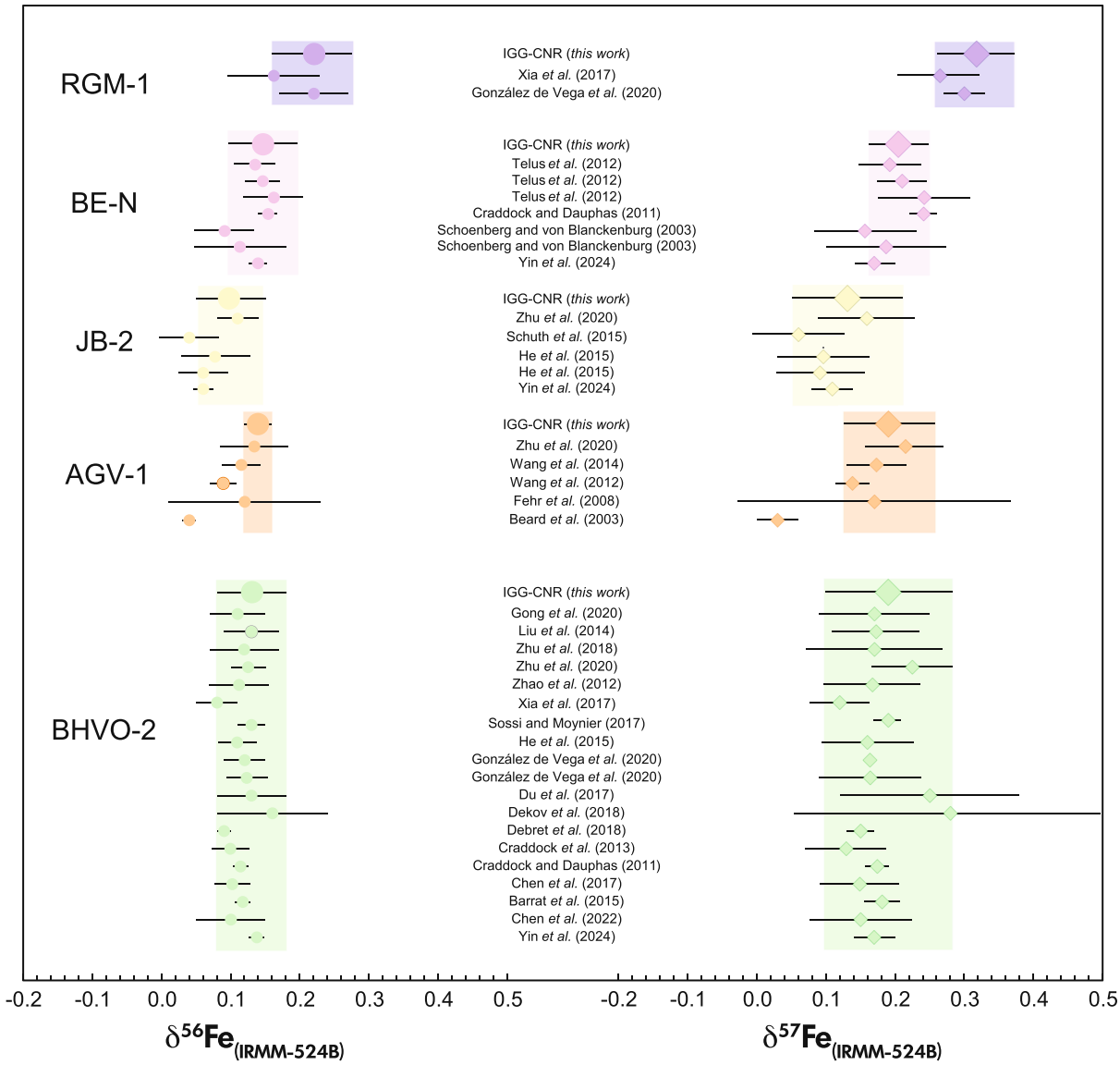

Figure 2. Summary of iron isotope (δ^{56}Fe and δ^{57}Fe) ratios of geological reference materials. Iron isotopic data obtained in this study (large symbols) were compared against literature data for the same samples (small symbols). 2*s* or 95% confidence levels are reported. All the literature data are reported in Table S2.

(2*s*) and 0.159 ± 0.066‰ (2*s*) reported by Zhu *et al.* (2020). The mean δ^{56}Fe and δ^{57}Fe values of BHVO-2 were 0.131 ± 0.047‰ (2*s*, n = 4) and 0.187 ± 0.092‰ (2*s*, n = 4), respectively, which are coherent those observed in the literature (Liu *et al.* 2014, Barrat *et al.* 2015, Sossi and Moynier 2017, Du *et al.* 2017, Zhu *et al.* 2020). BE-N sample is quite similar to previous materials, showing a mean δ^{56}Fe and δ^{57}Fe of 0.148 ± 0.044‰ (2*s*, n = 4) and 0.206 ± 0.044‰ (2*s*, n = 4), respectively, which are in good agreement with the values measured by Telus *et al.* (2012) and most recently Yin *et al.* (2024). Andesitic rock AGV-1 is in the same range of basaltic rocks with mean δ^{56}Fe and δ^{57}Fe of 0.141 ± 0.016‰ (2*s*, n = 5) and 0.189 ± 0.065‰ (2*s*, n = 5), with values very close to those obtained by Wang *et al.* (2014) and Zhu *et al.* (2020). Rhyolitic powder RGM-1 shows higher values in δ^{56}Fe and δ^{57}Fe, when compared with the other rocks, with δ^{56}Fe and δ^{57}Fe values of 0.221 ± 0.057‰ (2*s*, n = 5) and 0.324 ± 0.056‰ (2*s*, n = 5), respectively, resembling the values reported by Gonzales de Vega *et al.* (2020).

Figure 3 displays a linear trend (slope of 1.498, R^2 = 0.997) among the mean values of reference materials, which is very similar to measured isotopic mass-dependent fractionation trends in natural samples (1.466, Malinovsky

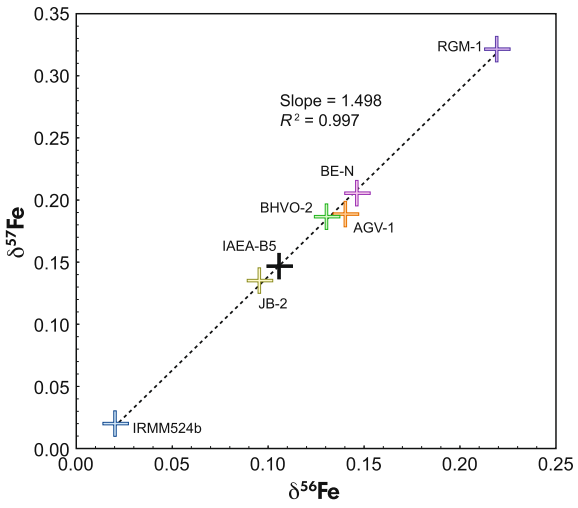

Figure 3. Mass fractionation in three-isotope diagram of Fe measured for geological reference materials. Data are also reported in Table 2 (Di Giuseppe *et al.* 2025).

et al. 2003, Craddock and Dauphas 2011), and closely overlaps the theoretical equilibrium (1.475) and kinetic (1.488) fractionation slopes. Comparison with literature data and linear trends obtained by reference materials confirms the reliability of the analytical methods employed in this study.

IAEA-B5: new recommended value for Fe isotope composition

Reference material IAEA-B5 is a powder rock derived from porphyritic basalt that erupted on July 22, 1998, from Etna Volcano main crater, in Sicily (Italy). Generally, this rock sample is used as stable isotope reference material as reported by Tonarini *et al.* (2003) for boron and Liu *et al.* (2018) for lithium isotopes. Our reasons for promoting and measuring the Fe isotopic composition of this rock are twofold: (i) the need for reference materials given the great demand for them in all laboratories around the world, driven

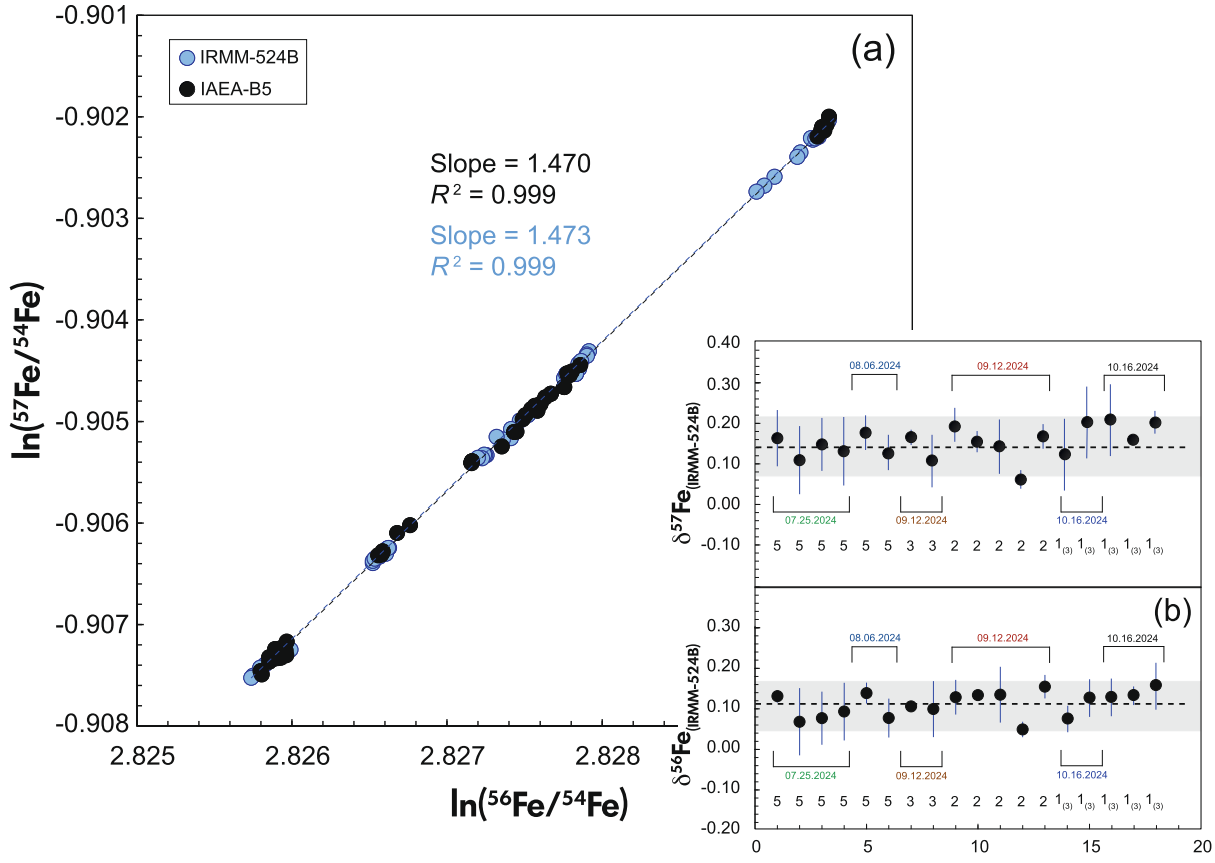

Figure 4. Results of fifty-one repeated analyses in six different measurement sessions of reference material IAEA-B5. (a) Three-isotope diagram reporting the ratios of IAEA-B5 and the same isotope ratio of IRMM-524b performed during the same measurement sequences. (b) δ^{56}Fe and δ^{57}Fe of IAEA-B5. Grey rectangles represent the mean values ± errors for each delta values.

by the rapid expansion of high-precision mass spectrometry instrumentation in the last twenty years, (ii) Being easily available at a low cost through the IAEA, this reference material can be used to promote intercalibration among laboratories worldwide. Furthermore, as illustrated in Figure S3, the selection of IAEA B5 is supported by its distinct composition (e.g., MgO *vs.* Fe_2O_3), compared with the other selected reference materials.

The isotopic Fe data obtained in this study for IAEA-B5 basaltic rock are presented in a three-isotope plot, plotting $\ln(^{56}Fe/^{54}Fe)$ against $\ln(^{57}Fe/^{54}Fe)$ as shown in Figure 4a, and compared with the regression slope of Fe reference material IRMM-524b analysed in the same measurement sessions. Both IAEA-B5 and IRMM-524b displayed indistinguishable slopes, yielding linear trends of 1.470 ($R^2 = 0.999$) and 1.473 ($R^2 = 0.999$), respectively, aligning with the theoretical values of kinetic and equilibrium fractionation lines (kinetic slope = 1.488, equilibrium slope = 1.475), as well as previously measured isotopic mass-dependent fractionation trends (slope = 1.466) in natural samples. Minor deviations from theoretical slopes could be due to external factors such as pressure, humidity, temperature or instrumental factors (unstable plasma conditions and resolution power), which influence the instrumental drift during long analytical sessions. For this reason, even though instrumental tuning is crucial, some external parameters remain uncontrollable. Table 2 and Figure 4b summarise the performed analyses relative to IAEA-B5 sample. The replicates of IAEA B-5 gave a mean of $\delta^{56}Fe$ and $\delta^{57}Fe$ of 0.105 ± 0.061 (2*s*, *n* = 17) and 0.147 ± 0.071 (2*s*, *n* = 17), respectively, that are in the range of the results obtained performing iron isotope compositions of previously described basaltic samples. The good agreement with other basaltic samples is also shown in Figure 3.

Conclusions

In this study, we propose new Fe isotope ratio reference values for the IAEA-B5 basalt, which is already used as B and Li isotope reference material. To validate the analytical quality of the values proposed, we first measured the Fe isotope ratios of widely used basaltic to rhyolitic reference materials, obtaining results consistent with published values from laboratories worldwide. After verifying the quality of the analysis against data published in the literature, we then measured the Fe isotope ratio of IAEA-B5. In this light, we propose $\delta^{56}Fe = 0.105 \pm 0.061$ (2*s*) and $\delta^{57}Fe = 0.147 \pm 0.071$ (2*s*) as recommended values for IAEA-B5.

Considering that the characterisation of the isotopic ratio as reference material ideally requires data from multiple laboratories, employing different measurement techniques and instrumentation, with the aim to minimise potential bias, we encourage the scientific community to regard these values as a starting point for future intercalibration between laboratories, and potentially offer an alternative to existing Fe reference materials.

Acknowledgements

PDG and SA acknowledge the support EU-Next Generation EU Mission 4 'Education and Research'-Component 2: 'From research to business'-Investment 3.1: 'Fund for the realization of an integrated system of research and innovation infrastructures'-Project IR0000032 - ITINERIS - Italian Integrated Environmental Research Infrastructures System-CUP B53C22002150006. Part of this research was funded by Italian Ministry of University and Research, grant number PRIN-MUR 2017AK8C32, TEOREM – Deciphering Geological Processes using Terrestrial and Extraterrestrial Ore Minerals, and by the National Plan of Recovery and Resilience (PNRR), funded by the European Union – Next Generation EU, Mission 4, Component 1, CUP B53D23007610006, Project PRIN-MUR 2022Y4J7AN - EUREECA - Rare Earth Elements in Urban and Mining Areas: an Emerging Concern for Soil (and Human) Health. Federico Farina is thanked for XRF analyses. Ilia Rodushkin is also thanked for fruitful discussion. Finally, we thank the two anonymous reviewers for their comments, which contributed to improving the manuscript.

Scientific editing by Jan Fietzke. Open access publishing facilitated by Consiglio Nazionale delle Ricerche, as part of the Wiley - CRUI-CARE agreement.

Data availability statement

All data generated or analysed during this study are included in the supporting information and the Data Repository available in Di Giuseppe *et al.* (2025).

References

Albarède F. and Beard B.L. (2004)
Analytical methods for non-traditional isotopes. In: Johnson C.M., Beard B.L. and Albarède F. (eds), Geochemistry of non-traditional isotopes. Reviews in Mineralogy and Geochemistry, 55. Mineralogical Society of America and Geochemical Society (Washington DC), 113–152.

Anbar A.D. (2004)
Iron stable isotopes: Beyond biosignatures. Earth and Planetary Science Letters, 217, 223–236.

Arnold G.L., Weyer S. and Anhar A.D. (2004)
Fe isotope variations in natural materials measured using high mass resolution multiple collector ICP-MS. Analytical Chemistry, 76, 322–327.

Beard B.L., Johnson C.M., Skulan J.L., Nealson K.H., Cox L. and Sun H. (2003)
Application of Fe isotopes to tracing the geochemical and biological cycling of Fe. Chemical Geology, 195, 87–117.

Beard B.L. and Johnson C.M. (2004)
Fe isotope variations in the modern and ancient Earth and other planetary bodies. Reviews in Mineralogy and Geochemistry, 55, 319–357.

Barrat J.-A., Rouxel O., Wang K., Moynier F., Yamaguchi A., Bischoff A. and Langlade J. (2015)
Early stages of core segregation recorded by Fe isotopes in an asteroidal mantle. Earth and Planetary Science Letters, 419, 93–100.

Belshaw N.S., Zhu X.K., Guo Y. and O'Nions R.K. (2000)
High precision measurement of iron isotopes by plasma source mass spectrometry. International Journal of Mass Spectrometry, 197, 191–195.

Chen K.Y., Liang P., Yuan H.L., Bao Z.A. and Chen L. (2017)
Improved nickel-corrected isotopic analysis of iron using high-resolution multi-collector inductively coupled plasma-mass spectrometry. International Journal of Mass Spectrometry, 421, 196–203.

Chernonozhkin S.M., Costas-Rodríguez M., Claeys P. and Vanhaecke F. (2017)
Evaluation of the use of cold plasma conditions for Fe isotopic analysis via multi-collector ICP-mass spectrometry: Effect on spectral interferences and instrumental mass discrimination. Journal of Analytical Atomic Spectrometry, 32, 538–547.

Craddock P.R. and Dauphas N. (2011)
Iron isotopic composition of geological reference materials and chondrites. Geostandards and Geoanalytical Research, 35, 101–123.

Dauphas N., Janney P.E., Mendybaev R.A., Wadhwa M., Richter F.M., Davis A.M., Van Zuilen M., Hines R.R. and Foley C.N. (2004)
Chromatographic separation and multicollection-ICP-MS analysis of iron. Investigating mass-dependent and -independent isotope effects. Analytical Chemistry, 76, 5855–5863.

Dauphas N., Pourmand A. and Teng F.Z. (2009)
Routine isotopic analysis of iron by HR-MC-ICP-MS: How precise and how accurate? Chemical Geology, 267, 175–184.

Dauphas N., John S.G. and Rouxel O. (2017)
Iron isotope systematics. Reviews in Mineralogy and Geochemistry, 82, 415–510.

Di Giuseppe P., Vezzoni S., Iannini Lelarge S., Rielli A., Agostini S. and Dini A. (2025)
High-precision iron isotopic analysis of IAEA-B5 basalt and rock reference materials. GFZ Data Services. https://doi.org/10.5880/fidgeo.2025.040

Du D-H., Wang X.-L., Tang T., Chen X., Li J.-Y. and Li W. (2017)
Origin of heavy Fe isotope compositions in high-silica igneous rocks: A rhyolite perspective. Geochimica et Cosmochimica Acta, 218, 58–72.

Fantle M.S. and Bullen T.D. (2009)
Essentials of iron, chromium, and calcium isotope analysis of natural materials by thermal ionization mass spectrometry. Chemical Geology, 258, 50–64.

Finlayson V.A., Konter J.G. and Ma L. (2015)
The importance of a Ni correction with ion counter in the double spike analysis of Fe isotope compositions using a $^{57}Fe/^{58}Fe$ double spike. Geochemistry, Geophysics, Geosystems, 16, 4209–4222.

Gong H., Guo P., Chen S., Duan M., Sun P., Wang X. and Niu Y. (2020)
A re-assessment of nickel-doping method in iron isotope analysis on rock samples using multi-collector inductively coupled plasma mass spectrometry. Acta Geochimica, 39, 355–364.

González de Vega C., Chernonozhkin S.M., Grygorian R., Costas-Rodríguez M. and Vanhaecke F. (2020)
Characterization of the new isotopic reference materials IRMM-524A and ERM-AE143 for Fe and Mg isotopic analysis of geological and biological samples. Journal of Analytical Atomic Spectrometry 35, 2517–2529.

He Y., Ke S., Teng F-Z., Wang T., Wu H., Lu Y. and Li S. (2015a)
High-precision iron isotope analysis of geological reference materials by high-resolution MC-ICP-MS. Geostandards and Geoanalytical Research, 39, 341–356.

He Y.S., Hu D.P. and Zhu C.W. (2015b)
Progress of iron isotope geochemistry in geoscience. Frontiers in Earth Science, 22, 54–71.

Johnson C.M. and Beard B.L. (1999)
Correction of instrumentally produced mass fractionation during isotopic analysis of Fe by thermal ionization mass spectrometry. International Journal of Mass Spectrometry, 193, 87–99.

Johnson C.M., Beard B.L. and Albarède F. (editors) (2004)
Geochemistry of non-traditional isotopes. Reviews in Mineralogy and Geochemistry, 55. Mineralogical Society of America and Geochemical Society (Washington DC), 454pp.

references

Johnson C.M., Skulan J.L., Beard B.L., Sun H. Nealson K.H. and Braterman P.S. (2002)
Isotopic fractionation between Fe(III) and Fe(II) in aqueous solutions. Earth and Planetary Science Letters, 195, 141–153.

Kehm K., Hauri E.H., Alexander C.M.O.D. and Carlson R.W. (2003)
High precision iron isotope measurements of meteoritic material by cold plasma ICP-MS. Geochimica et Cosmochimica Acta, 67, 2879–2891.

Liu S.-A., Li D., Li S., Teng F.-Z., Ke S., He Y. and Lu Y. (2014)
High-precision copper and iron isotope analysis of igneous rock standards by MC-ICP-MS. Journal of Analytical Atomic Spectrometry, 29, 122–133.

Liu Y.H., Huang K.-F. and Lee D.-C. (2018)
Precise and accurate boron and lithium isotopic determinations for small sample-size geological materials by MC-ICP-MS. Journal of Analytical Atomic Spectrometry 33, 846–855.

Malinovsky D., Stenberg A., Rodushkin I., Andren H., Ingri J., Ohlander B. and Baxter D.C. (2003)
Performance of high-resolution MC-ICP-MS for Fe isotope ratio measurements in sedimentary geological materials. Journal of Analytical Atomic Spectrometry, 18, 687–695.

Maréchal C.N., Télouk P. and Albarède F. (1999)
Precise analysis of copper and zinc isotopic compositions by plasma source mass spectrometry. Chemical Geology, 156, 251–273.

Millet M.A., Baker J.A. and Payne C.E. (2012)
Ultra-precise stable Fe isotope measurements by high resolution multiple-collector inductively coupled plasma mass spectrometry with a ^{57}Fe-^{58}Fe double spike. Chemical Geology, 624–305, 18–25.

Poitrasson F. and Freydier R. (2005)
Heavy iron isotope composition of granites determined by high resolution MC-ICP-MS. Chemical Geology, 222, 132–147.

Prohaska T., Irrgeher J., Benefield J., Böhlke J.K., Chesson L.A., Coplen T.B., Ding T., Dunn P.J.H., Gröning M., Holden N.E., Meijer H.A.J., Moossen H., Possolo A., Takahashi Y., Vogl J., Walczyk T., Wang J., Wieser M.E., Yoneda S., Zhu X.K. and Meija J. (2022)
Standard atomic weights of the elements 2021 (IUPAC Technical Report). Pure and Applied Chemistry, 94, 573–600.

Russell W.A., Papanastassiou D.A. and Tombrello T.A. (1978)
Ca isotope fractionation on the Earth and other solar system materials. Geochimica et Cosmochimica Acta, 42, 1075–1090.

Rouxel O., Dobbek N., Ludden J. and Fouquet Y. (2003)
Iron isotope fractionation during oceanic crust alteration. Chemical Geology, 202, 155–182.

Rudge J.F., Reynolds B.C. and Bourdon B. (2009)
The double spike toolbox. Chemical Geology, 265, 420–431.

Schoenberg R. and von Blanckenburg F. (2005)
An assessment of the accuracy of stable Fe isotope ratio measurements on samples with organic and inorganic matrices by high-resolution multicollector ICP-MS. International Journal of Mass Spectrometry, 242, 257–272.

Sossi P.A., Halverson G.P., Nebel O. and Eggins S.M. (2015)
Combined separation of Cu, Fe and Zn from rock matrices and improved analytical protocols for stable isotope determination. Geostandards and Geoanalytical Research, 39, 129–149.

Sossi P.A. and Moynier F. (2017)
Chemical and isotopic kinship of iron in the Earth and Moon deduced from the lunar Mg-Suite. Earth and Planetary Science Letters, 471, 125–135.

Strelow F.E.W. (1980)
Improved separation of iron from copper and other elements by anion-exchange chromatography on a 4% cross-linked resin with high concentrations of hydrochloric acid. Talanta, 27, 727–732.

Telus M., Dauphas N., Moynier F., Tissot F.L.H., Teng F.-Z., Nabelek P.I., Craddock P.R. and Groat L.A. (2012)
Iron, zinc, magnesium and uranium isotopic fractionation during continental crust differentiation: The tale from migmatites, granitoids and pegmatites. Geochimica et Cosmochimica Acta, 97, 247–265.

Teng F.-Z., Dauphas N. and Watkins J.M. (2017)
Non-traditional stable isotopes: Retrospective and prospective. Reviews in Mineralogy and Geochemistry, 82, 1–26.

Tonarini S., Pennisi M., Adorni-Braccesi A., Dini A., Ferrara G., Gonfiantini R., Wiedenbeck M. and Gröning M. (2003)
Intercomparison of boron isotope and concentration measurements. Part I: Selection, preparation and homogeneity tests of the intercomparison materials. Geostandards Newsletter: The Journal of Geostandards and Geoanalysis, 27, 21–39.

Völkening J. and Papanastassiou D.A. (1989)
Iron isotope anomalies. Astrophysical Journal, 347, L43–L46.

Von Blanckenburg F., Mamberti M., Schoenberg R., Kamber B.S. and Webb G.E. (2008)
The iron isotope composition of microbial carbonate. Chemical Geology, 249, 113–128.

Wang K., Savage P.S. and Moynier F. (2014)
The iron isotope composition of enstatite meteorites: Implications for their origin and the metal/sulfide Fe isotopic fractionation factor. Geochimica et Cosmochimica Acta, 142, 149–165.

references

Weyer S. and Schwieters J.B. (2003)
High precision Fe isotope measurements with high mass resolution MC-ICP-MS. **International Journal of Mass Spectrometry, 226**, 355–368.

Yin N.-H., Louvat P., Preud'homme H., Ronzani A.-L., Ash J., Berail S. and Amouroux D. (2024)
Precise measurement of Fe isotopes in marine and biological samples by pseudo-high-resolution multi-collector inductively coupled plasma-mass spectrometry (MC-ICP-MS). **Analytical and Bioanalytical Chemistry, 416**, 4153–4171.

Zhu X.K., O'Nions R.K., Guo Y. and Reynolds B.C. (2000)
Secular variation of iron isotopes in north Atlantic deep water. **Science, 287**, 2000–2002.

Zhu X.K., Guo Y., Williams R.J.P., O'Nions R.K., Matthews A., Belshaw N.S., Canters G.W., de Waal E.C., Weser U., Burgess B.K. and Salvato B. (2002)
Mass fractionation processes of transition metal isotopes. **Earth and Planetary Science Letters, 200**, 47–62.

Zhu C., Lu W., He Y., Ke S., Wu. and Zhang L. (2018)
Iron isotopic analyses of geological reference materials on MC-ICP-MS with instrumental mass bias corrected by three independent methods. **Acta Geochemica 37**, 691–700.

Zhu G., Ma J., Wei G. and An Y. (2020)
A novel procedure for separating iron from geological materials for isotopic analysis using MC-ICP-MS. **Journal of Analytical Atomic Spectrometry 35**, 873–877.

Supporting information

The following supporting information may be found in the online version of this article:

Figure S1. Photograph of columns used for chemical purification.

Figure S2. Typical Faraday cup positions relative to the masses selected for measurement.

Figure S3. MgO vs. Fe_2O_3 diagram of selected samples.

Table S1. Mean major and trace element compositions of reference material IAEA-B5.

Table S2. Column chromatography procedure using AG1-X8 (200–400 mesh) resins and 0.4 × 7 cm PTFE columns.

Table S3. Comparison between IGG-CNR Pisa Laboratory measurement results and literature values.

This material is available from: http://onlinelibrary.wiley.com/doi/10.1111/ggr.70017/abstract (This link will take you to the article abstract).